THE JOURNAL OF PHYSICAL CHEMISTRY C

Article

pubs.acs.org/JPCC

Post-Synthesis Conversion of Borosilicate Zeolite Beta to an Aluminosilicate with Isolated Acid Sites: A Quantitative Distance Analysis by Solid-State NMR

Hubert Koller,*[,†] Soumya Senapati,[†] Jinjun Ren,[†] Tobias Uesbeck,[†] Vassilios Siozios,[†] Michael Hunger,[‡] and Raul F. Lobo[§]

[†]Institute of Physical Chemistry, University of Münster, Corrensstrasse 28/30, 48149 Münster, Germany

[‡]Institute of Chemical Technology, University of Stuttgart, 70550 Stuttgart, Germany

[§]Center for Catalytic Science and Technology, Department of Chemical and Biomolecular Engineering, University of Delaware, Newark, Delaware 19716, United States

Supporting Information

ABSTRACT: Isolated acid sites were selectively generated by postsynthesis modification of a borosilicate zeolite beta. To this end, samples were prepared with pairs of adjacent boron sites balanced by Ca^{2+} ions, whereas isolated boron in the zeolite framework was balanced by NH_4^+ ions. To avoid undesired boron leaching, these ion exchange reactions were carried out in methanol solution rather than in water. Trigonal boron forms near the NH_4^+ ions by decomposing the latter into NH_3 (and a proton), and selective extraction of the trigonal boron is achieved by water treatment, whereas the tetrahedral boron near Ca^{2+} ions remains in the zeolite framework. The vacancies were refilled with aluminum by treatment with an aqueous $Al(NO_3)_3$ solution. Two Brønsted acid sites with ^1H chemical shifts of 4.0 and 5.0 ppm exist in the dehydrated samples. $^1H-^{27}Al$ REAPDOR solid-state NMR measurements yield quantitative information on the local H−Al distances of isolated H−Al two-spin and H−Al−Al three-spin systems. The nearest H−Al distance is determined at 2.50 Å with an accuracy of 2% (or better) by fitting the oscillatory part of the REAPDOR curves, which was not observed before for zeolite acid sites. The second nearrest Al neighbors show a much larger distance of about 5 Å for the acid protons with a chemical shift of δ = 4 ppm. A second acid site at δ = 5 ppm has an approximately 50% occupation of a second Al neighbor at 3.73 Å, possibly within the same six-ring. This high resolution of dipolar interaction is not observed in a standard zeolite Al-beta prepared by direct synthesis. The method is suitable to identify well-defined local ordering in Al distributions of zeolites.

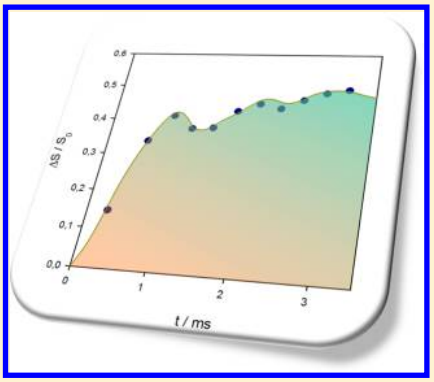

1. INTRODUCTION

The classical method to prepare Brønsted acid sites in zeolites is to exchange NH_4^+ for other ions in the zeolite pores (such as alkali ions) in an aqueous ion exchange process and subsequently thermally decompose the ammonium ion into NH_3 and a proton. The Brønsted proton, H^+, binds to a bridging oxygen that is connected to a trivalent atom in tetrahedral framework position, $TO_{4/2}^-$, thus ensuring charge neutrality.[1−4] The most common trivalent (tetrahedral) T atom in Brønsted acid sites is Al, but Ga, B, or other trivalent ions are also possible. Nonetheless, this simple bridging hydroxyl model of an acid site is usually insufficient to explain differences in catalytic properties of different zeolite materials.

Zeolite catalysts are highly complex, and the most important factors affecting their properties may be classified as follows: (i) Shape selectivity,[5−8] a topological property that allows the material to discriminate between the size of different reactants, products, or transition states in a catalytic reaction thereby controlling what enters, leaves, or forms within the pore system of zeolites. (ii) Acidity,[9] a measure of the ability of an acid site to donate a proton to an adsorbed species, which in turn depends on at least two parameters: (a) the gas-phase deprotonation energy of the bridging hydroxyl groups and (b) the adsorption energy of the protonated base.[10−12] The deprotonation energy is only amenable by quantum−chemical calculations, whereas the adsorption of a base is quantifiable using a variety of experimental methods.[13,14] The density of framework Al affects the deprotonation energy and catalytic performance of bridging hydroxyl groups.[2] (iii) Steric effects such as gradients in catalytic site density and diffusion control (depending on crystal size) and other macrokinetic effects[15] can affect zeolite catalysis.[16,17]

Given the complex set of parameters affecting the catalytic properties of zeolites, the synthesis control of catalytic site density and site location is of significant relevance.[18] A combined study using ^{27}Al solid-state NMR and quantum−

Received: February 18, 2016
Revised: April 13, 2016
Published: April 14, 2016

ACS Publications © 2016 American Chemical Society

DOI: 10.1021/acs.jpcc.6b01680
J. Phys. Chem. C 2016, 120, 9811−9820

chemical methods on ZSM-5 has demonstrated the importance of synthesis variables on Al site locations.[19,20] In addition, the presence of Al next-nearest (Al−O−Si−O−Al) and next-next-nearest (Al−O−Si−O−Si−O−Al) tetrahedral neighbors change the local geometry of $AlO_{4/2}^-$ tetrahedra, which changes the ^{27}Al chemical shifts by up to 4 ppm.[20] However, high-resolution ^{27}Al solid-state NMR in these studies was carried out on hydrated samples. Dehydrated acid zeolite catalysts show an extreme broadening of the ^{27}Al line due to a large quadrupolar coupling of the severely distorted $AlO_{4/2}^-$ tetrahedra,[12,21] and conventional magic angle spinning does not allow us to acquire a signal at all. High-resolution ^{27}Al solid-state NMR of zeolites in their catalytically active and dehydrated form require special techniques for signal detection. Kentgens et al. for instance obtained line narrowing by DFS-enhanced ^{27}Al MQMAS NMR spectroscopy on ZSM-5, a technique in which ^{27}Al excitation was carried out by a double-frequency sweep.[22] These studies illustrate that there is a demand for methods of synthesis control on the location of catalytic sites along with suitable characterization techniques of site locations and densities.

The incorporation of Al in high-silica zeolites can be influenced by synthesis parameters in the hydrothermal reaction.[23] The insertion of heteroatoms in hydrothermal synthesis appears to be different for different elements. Although many zeolites allow the (comparatively flexible) insertion of a range of aluminum concentrations, the tolerance for boron insertion seems to be more restricted. However, borosilicate zeolites show distinct properties,[24] making them interesting for postsynthesis modifications.[4,25−27] In addition, boron appears to prefer to be placed in special crystallographic T sites more selectively than Al.[28−30] Therefore, borosilicate zeolites that are converted to their aluminum form by replacing boron bear considerable potential for catalytic properties that are distinct from aluminosilicate zeolites made by direct synthesis. Moreover, postsynthesis Al/B exchange offers additional opportunities to create a selective Al site distribution. In our previous report, we identified a set of control parameters that allow the postsynthesis substitution of boron by aluminum with tailored extent of exchange.[31] This method is based on the differential reactivity of boron atoms in the zeolite framework, depending on the counterion. Tetrahedral boron ($BO_{4/2}^-$) exists in the neighborhood of cations that have weak binding to the zeolite framework such as alkali cations, whereas trigonal framework boron ($BO_{3/2}$) forms when a proton replaces an alkali ion and binds to one of the four oxygens of $BO_{4/2}^-$ sites. The protonated oxygen forms a silanol group, the B−O bond is broken, and boron coordination becomes trigonal. Trigonal boron can easily be extracted from the framework by a hydrolytic reaction with water in a slightly acidic environment, whereas tetrahedral boron remains stable in the framework. The extracted boron is believed to leave a so-called hydroxyl nest with four silanol groups surrounding a T vacancy. This vacancy can be refilled with a T atom, such as Al or others.[25,26,31,32] To achieve stoichiometric control of the extent of B/Al substitution by mixed H^+/alkali counterions, special precautions have to be taken to avoid that the acidic properties of aqueous Al^{3+} solutions remove the alkali ions by ion exchange. Al should only enter the T vacancies left by the extracted trigonal boron, while leaving tetrahedral $BO_{4/2}^-$/alkali sites unaffected. Tong and Koller used alcoholic instead of aqueous solutions to achieve a high selectivity of B/Al substitution in favor of those sites balanced by a proton and leaving the boron near a Na^+ cation untouched.[31] Note that alcohols do not develop acidic protons in the presence of Al^{3+} as H_2O does. Zeolite beta is superior for such B/Al exchange studies. It allows a relatively high amount of boron to be placed in the framework by direct synthesis. Additionally, it is a large-pore zeolite (12-membered ring channels) for which the transport of exchanging $Al(H_2O)_6^{3+}$ ions is easily possible, whereas their diffusion in 10-membered (or smaller) rings is restricted.[33]

In this work, we focus on two aspects of zeolite beta materials: (1) Samples were prepared following different synthesis approaches to control the location and site densities of active sites. (2) We used solid-state NMR to probe the local environment of a zeolite Brønsted proton in an intermediate range of up to 1 nm so that local pairing can be identified on the basis of $^1H−^{27}Al$ and $^1H−^{27}Al−^{27}Al$ dipolar interactions. It is shown that the local site densities of zeolite beta strongly depend on its synthesis. Particular emphasis in the synthesis part is laid on the postsynthesis replacement of boron by aluminum in the zeolite framework. NMR spectroscopy is used to determine the local structure of Brønsted acid sites and compare the distribution of catalytic sites between different synthesis procedures.

2. EXPERIMENTAL SECTION

2.1. Materials. The synthesis steps are summarized in Scheme 1. B-beta (structure-type code BEA) of route A was made with tetraethylammonium cations, TEA^+, according to a procedure published elsewhere.[34] The gel composition was 1

Scheme 1. Reaction Sequences to Synthesize Aluminated Zeolite Beta Samples after Partial Deboronation or by Direct Synthesis[a]

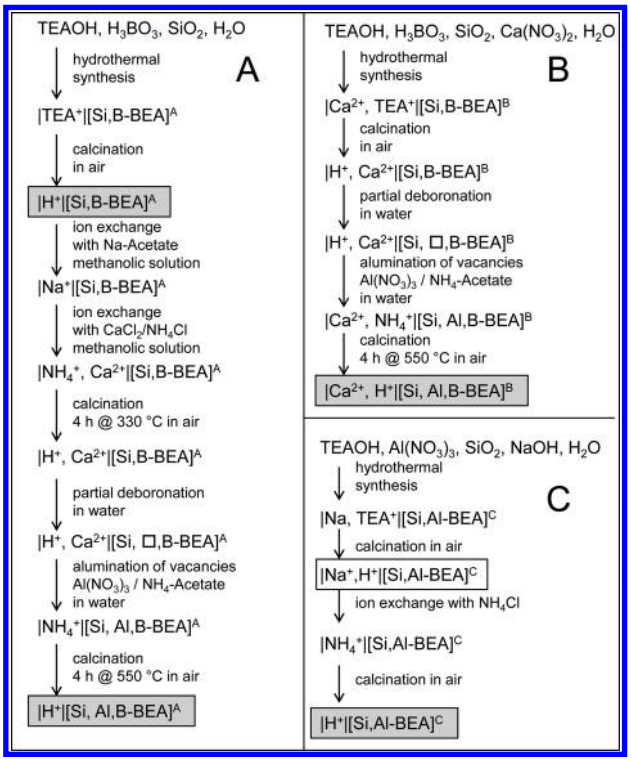

[a] □ stands for generated vacancies.

DOI: 10.1021/acs.jpcc.6b01680
J. Phys. Chem. C 2016, 120, 9811−9820

SiO_2/0.033 B_2O_3/0.54 TEAOH/18 H_2O. It should be mentioned that this synthesis does not contain sodium cations.

For route B, a modified synthesis was carried out in the presence of Ca^{2+} ions. In 154 mL of an aqueous TEAOH solution (20% w/w, Acros Organics) and 3 mL of deionized water, 1.63 g of (0.026 mol) H_3BO_3 (Aldrich) was dissolved. The solution was stirred for 30 min to allow the boric acid to be dissolved, and then 0.6565 g of $Ca(NO_3)_3.4H_2O$ (0.0028 mol) were added to the mixture. The solution became turbid because of the formation $Ca(OH)_2$, but the calcium was detected in the final zeolite product (by elemental analysis of the zeolite). After that, 24.03 g of Cab-O-Sil M5 (Cabot) was slowly added, and the gel was stirred for 2 h. Then, a little amount of boron beta zeolite crystals was added as seeding crystals, and the gel was stirred for 4 h to obtain a homogeneous gel, which was charged in Teflon-lined stainless-steel autoclaves and heated at 423 K. The crystallizations were typically completed after 96 h. Then, the reaction was quenched with cold water. The solid phase was separated by filtration and washed with an adequate amount of water until pH ∼9. The crystals were dried at 323 K overnight.

The Al-beta sample of route C was hydrothermally synthesized with a gel composition of 1 SiO_2/0.033 Al_2O_3/0.1 Na_2O/0.54 TEAOH/19 H_2O. To 50 mL of TEAOH (20 wt % in H_2O, Aldrich) was added 3.25 g of $Al(NO_3)_3{\cdot}9H_2O$ dissolved in 5 mL of H_2O. Then, 1.05 g of NaOH were added after 30 min, and the solution was stirred for 1 h. Afterward, 8.0 g of fumed silica (Aldrich, 0.007 μm) were slowly added to allow sufficient dissolution of the silica before the mixture became too viscous. The gel was aged for 4 h and then heated in a Teflon-lined steel autoclave at 423 K for 8 days. The solid product was washed with deionized water until pH 9 and dried overnight at 323 K.

Calcination of as-synthesized B-beta zeolite was carried out in air by heating from room temperature to 923 K in a muffle furnace. The heating rate was 2 K/min, and the temperature was held at two points (383 and 693 K) for 2 h each. The final temperature was maintained for 6 h. Al-beta zeolites were calcined at 823 K for 8 h by using a ramp of 3 K/min.

Calcined B-beta zeolite was ion-exchanged with sodium to replace all the protons with sodium; 1 g of calcined B-beta zeolite was added to 50 mL of 1.5 M methanolic solution of sodium acetate. The solution was stirred at room temperature for 24 h, and then it was filtered and washed several times with methanol. This process was repeated twice.

Mixed Ca^{2+}/NH_4^+ ion exchange was carried out for 24 h with 0.5 g of zeolite and 50 mL of 1.12 M methanolic solutions. After that, the solid zeolite powders were separated by filtration and washed several times with methanol to remove the excess calcium chloride or ammonium chloride. The solids were dried at 323 K overnight.

Deboronation was carried out with 100 mL of deionized water per gram of the B-beta zeolites at room temperature. The mixtures were stirred slowly for 12 h, separated by filtration and dried at 323 K overnight. This process was repeated four times for complete deboronation of the protonated sites. Alumination of the deboronated zeolites were carried out by aqueous solution of aluminum nitrate. The aluminum solution was prepared by dissolving 0.5 g of $Al(NO_3)_3{\cdot}9H_2O$ in 200 mL of deionized water. Then, 0.892 g of ammonium acetate was added to the solution to increase the pH of the solution. The final pH of the solution was 6. Deboronated sample (500 mg) was added in 100 mL of aluminum nitrate solution and stirred for 24 h at room temperature. Solid zeolite samples were separated by filtration and washed with adequate amount of water to remove the physisorbed aluminum nitrate.

Dehydration of the acid form was carried out in glass ampules for 12 h in vacuum with a final temperature of 723 K. The heating rate was 2 K/min with a stop at 393 K for 2 h.

2.2. Analyses. The powder X-ray diffraction of zeolites was carried out on a Guinier-Camera, using Cu Kα_1 radiation (λ = 1.5406 Å). All the measurements were carried out with 33 min exposure time. The data were acquired between 7 and 50° (2θ), with 0.025° step. The samples were prepared as thin layers on an amorphous scotch tape, prior to scanning. Chemical analyses were carried out by ICP-OES. To determine the number density of acid sites, isopropylamine (IPA) was adsorbed on the samples.

The interaction of IPA with the zeolite surface and the evaluation of the ratio between weak and strong Brønsted acid sites were carried out by TGA-MS investigations, TGA Q5000-IR thermogravimetric analyzer from TA Instruments, Inc., USA, coupled with a GSD 301 T3 ThermoStar gas analysis system from Pfeiffer Vacuum GmbH. To this end, 10 mg of sample was heated in the thermogravimetric analyzer to 623 K for 90 min in a He flow (35 mL/min) to achieve a constant sample weight caused by desorption of physisorbed water. After this drying step, the samples were cooled down to 303 K. The He flow was switched through the IPA storage vessel. After 10 min, the sample surface was saturated with IPA, and the TGA-MS system was purged free of IPA. The sample was heated at 2 K/min and desorbing species were analyzed online with a mass spectrometer.

Solid-state NMR experiments were carried out on a 400 MHz Bruker Advance spectrometer, equipped with a 4 mm MAS double-resonance probe that was operated at a spinning speed of 12.0 or 14.0 kHz. ^{1}H MAS NMR spectra were recorded using 90° pulses between 3.6 and 4.3 μs length and a relaxation delay between 8 and 15 s. Chemical shifts are reported relative to solid adamantane as a secondary reference (1.75 ppm). ^{27}Al MAS NMR spectra were recorded using short excitation pulses of 0.7 μs and a relaxation delay of 1 s. Chemical shifts are reported relative to a 1 M $Al(NO_3)_3$ aqueous solution. ^{11}B MAS NMR spectra were acquired at 160.5 MHz with the same number of scans for quantitative comparison. A probehead background was removed by baseline correction. ^{1}H−^{27}Al REAPDOR (rotational echo adiabatic passage double resonance) experiments were conducted with a rotor spinning frequency of 12.0 or 14.0 kHz. ^{1}H 90° pulses were typically between 3.6 and 4.5 μs (69 kHz and 55 kHz rf power), and the ^{27}Al recoupling pulse was set to 9 μs with an rf power between 55 and 52 kHz (as determined on the liquid $Al(NO_3)_3$ solution). A recycle delay between 8 and 15 s was applied, followed by a presaturation train of 15 π/2 pulses. Quantitative peak simulations were carried out with the program DMFIT.

Quantitative information on the ^{1}H−^{27}Al heteronuclear dipolar interactions was obtained by numerical simulations of the REAPDOR time evolution curves. The time evolution of the density matrix under the appropriate Hamiltonian, taking into account the pulse sequence and spin system, was simulated with the program SIMPSON.[35]

3. RESULTS AND DISCUSSION

3.1. Postsynthesis Methods. The synthesis approach to control the location and densities of acid sites in zeolite beta is shown in Scheme 1. Route A begins with the hydrothermal

DOI: 10.1021/acs.jpcc.6b01680
J. Phys. Chem. C 2016, 120, 9811−9820

synthesis of a borosilicate beta zeolite using tetraethylammonium cations as the structure directing agent. No alkali ions were added to the synthesis mixture in order to avoid high pore charge densities generated by these cations, thus forcing the bulkier tetraethylammonium cations (TEA^+) to be the only contributor to balance the framework charge density in the product. However, the absence of smaller alkali cations cannot be taken as a guarantee that a more or less equidistant distribution of $BO_{4/2}^-$ tetrahedra in the zeolite framework would be generated according to the packing density of charge-balancing TEA^+ cations. Therefore, additional measures were taken (see below) to analyze the amount of paired $BO_{4/2}^-$ sites and prevent the transformation of these pairs into paired Brønsted acid sites in the final product.

The obtained parent zeolite, $|TEA^+|[Si,B\text{-}BEA]^A$, has a Si/B ratio of 12, and it is first converted to the proton form by calcination, $|H^+|[Si,B\text{-}BEA]^A$. To avoid acidity generation during the additional modification reactions, in particular the well-known deboronation in liquid water, the H-form was first ion-exchanged to the sodium form. This exchange was carried out in a methanol solution to avoid deboronation, which would take place in an aqueous suspension. Then, a mixed ion exchange with NH_4^+ and Ca^{2+} ions was carried out, again in methanol, to replace all Na^+. Ion exchange isotherms were obtained by varying the $Ca^{2+}/(Ca^{2+}+NH_4^+)$ ratio, and the amounts of framework $BO_{4/2}^-$ sites charge balanced by Ca^{2+} were determined by Ca and B elemental analyses (Figure 1a). The S-type ion exchange isotherm indicates the existence of sites, which prefer the Ca^{2+} ions over the leaving Na^+ or competing NH_4^+ ions. These preferred sites are completely balanced by Ca^{2+} at a 50% ratio of Ca^{2+} and NH_4^+ in the exchange solution (Figure 1a). These paired $BO_{4/2}^-$ sites make up a total of about 7% of all framework boron. A sketch of possible pairing is shown in Figure 1b for six-rings of the zeolite framework structure, but pairing is not necessarily restricted to such rings. All further analyses were carried out with the sample at 50% ratio of NH_4^+ and Ca^{2+} in the ion exchange.

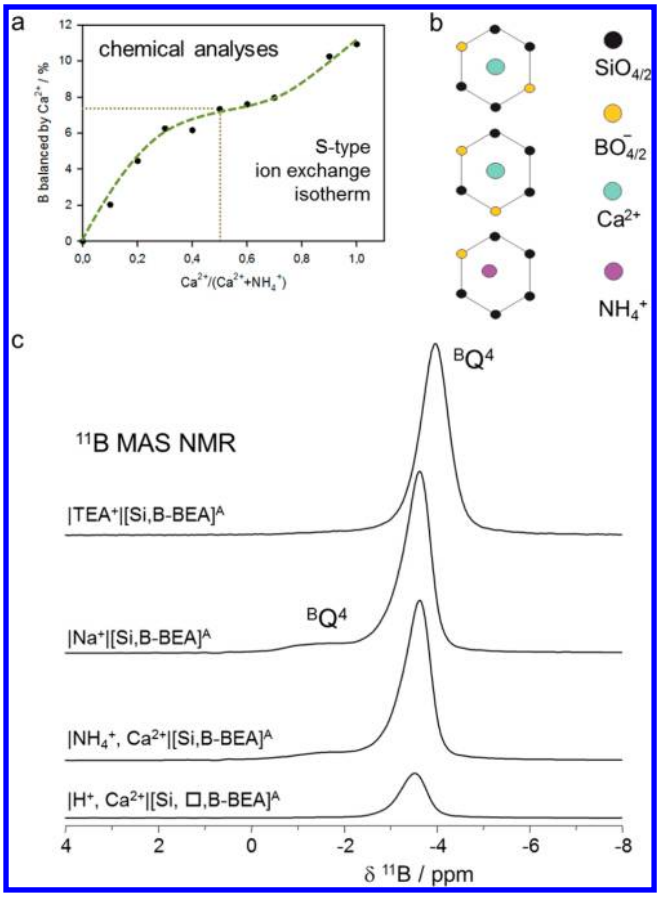

Figure 1. ^{11}B MAS NMR after various steps of treatment (□ is a vacancy defect).

Another calcination step converts this sample to $|H^+,Ca^{2+}|[Si,B\text{-}BEA]^A$. The purpose of the mixed ion exchange was also to balance pairs of framework charges of $BO_{4/2}^-$ by Ca^{2+} ions such that the isolated (nonpaired) charges are protonated. The proton binds covalently to the zeolite bridging oxygen near isolated boron, whereas the Ca^{2+} ions form an ionic interaction with the negative framework charge of two paired $BO_{4/2}^-$ tetrahedra. Protonation of the framework oxygen transforms the boron coordination to a trigonal $BO_{3/2}$ site with a neighboring SiOH group (i.e., the framework bridge is disrupted). This change in boron coordination number does not occur for the ionic interaction of Ca^{2+} at the paired sites. In this form, it is easy to extract boron from the isolated, protonated sites in an aqueous suspension, whereas the paired sites remain intact. The ^{11}B MAS NMR data in Figure 1c show that the initial postsynthesis step indeed keep boron in the framework ($^BQ^4$) until the purposeful deboronation step is carried out in the H^+/Ca^{2+} mixed-ion form. All spectra in Figure 1c show tetrahedral boron with a sharp drop in intensity upon boron removal. We also tentatively assign the small, broad peak near −2 ppm to $^BQ^4$.[26] The sample $Ca^{2+}|[Si,□,B\text{-}BEA]^A$ (□ stands for T vacancies) after deboronation still contains an amount of boron in the framework, which is consistent with the number of sites charge-balanced by Ca^{2+}.

In the alumination step of $|H^+,Ca^{2+}|[Si,□,B\text{-}BEA]^A$ the Ca^{2+} ions are also exchanged by NH_4^+ in the aqueous ammonium acetate buffer solution to give $|H^+|[Si,Al,B\text{-}BEA]^A$ after a final calcination. After these various postsynthesis steps, the sample is still crystalline (Figure S1), and its structural integrity and acid function will be further characterized below. This zeolite was prepared to obtain a sample with truly isolated acid sites via a borosilicate starting material.

Route B employs Ca^{2+} ions to balance paired sites right from the beginning in the hydrothermal synthesis. Although it was not necessarily expected that a crystalline beta zeolite would be obtained in the presence of Ca^{2+}, the sample was sufficiently crystalline and also stable in the postsynthesis steps. Again, boron was replaced by aluminum by postsynthesis reactions (Scheme 1).

Sample C is a reference zeolite beta for which aluminum was inserted into the framework directly by hydrothermal synthesis. After calcination, this material is subjected to an NH_4^+ ion exchange to replace the Na^+ ions which originate from NaOH in the synthesis gel. Powder X-ray diffraction data of samples made by routes B and C are shown in Figure S2. Figure 2 compares the ^1H MAS NMR spectra of the dehydrated proton forms of three zeolites: $|H^+|[Si,Al,B\text{-}BEA]^A$ and $|Na^+,H^+|[Si,Al\text{-}BEA]^C$ as well as $|H^+|[Si,Al\text{-}BEA]^C$. The latter two are obtained before and after NH_4^+ ion exchange of sample C. All spectra show the two well-known lines for Brønsted acid sites at 4 and 5 ppm,[36] along with several components for AlOH and SiOH groups with chemical shifts below 3 ppm.[13] The reason why there are two lines at 4 and 5 ppm for bridging hydroxyl groups is not yet fully understood. Most authors assign these lines to

DOI: 10.1021/acs.jpcc.6b01680
J. Phys. Chem. C 2016, 120, 9811−9820

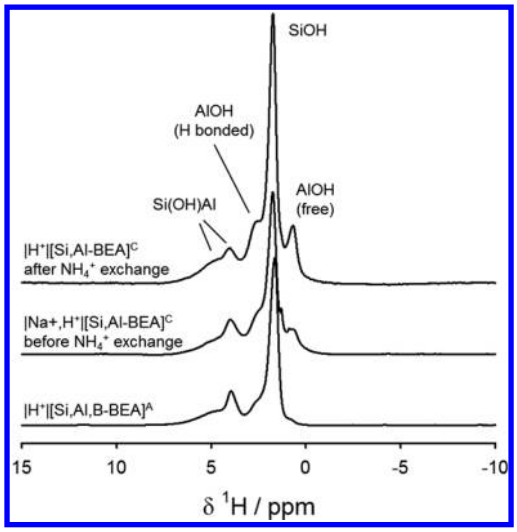

Figure 2. ^{1}H MAS NMR of various dehydrated samples.

unperturbed and perturbed (others use non-H-bonded and H-bonded) bridging hydroxyl groups. Interestingly, the relative contribution of perturbed (H-bonded) Brønsted acid sites is different for the three samples. It grows after exchange of remaining Na^+ ions by H^+. Quantitative simulation of peak intensities results in ratios between H-bonded an non-H-bonded acid sites of 4.3, 1.9, and 0.9 for $|H^+|[Si,Al\text{-}BEA]^C$, $|Na^+$, $H^+|[Si,Al\text{-}BEA]^C$, and $|H^+|[Si,Al,B\text{-}BEA]^A$, respectively. Therefore, the ratio is increased by about a factor of 2 when the sodium cations are ion-exchanged by NH_4^+ in sample C, showing that Na^+ ions in the synthesis produce a substantial portion of H-bonded acid sites after the postsynthesis conversion. We conclude that the organic (TEA^+) and inorganic (Na^+) cations do not produce the same distribution of acid sites. This is, to the best of our knowledge, the first ^{1}H NMR report that shows that the type of Brønsted proton is influenced by the counterion used in the hydrothermal synthesis. Sample A has the lowest amount of H-bonded acid sites. However, the same proton chemical shifts of Brønsted sites (lines at 4 and 5 ppm) are observed, no matter whether Al is directly inserted into the zeolite framework in hydrothermal synthesis or it is postsynthetically exchanged for boron.

The hydrogen-bonded acid site in ZSM-5 appears at 6.5 ppm,[37] and it was assigned to a bridging hydroxyl group in a five-membered ring of this zeolite.[38,39] Because the chemical shift of the H-bonded acid site is at 5 ppm in zeolite beta, it is suggested to be in a weaker H-bond (longer O−O distance), and we conclude that it may be located in a six-ring rather than a five ring. Beck and Haw have shown that there is no motion of the protons at room temperature in zeolite beta.[36] Careful sample dehydration is required for such studies to avoid vehicle hopping of the protons with residual water.[40] It is important to rule out any motional effects for the purpose of measuring the H−Al distances in zeolites.[41,42]

Selected ^{29}Si MAS NMR spectra of samples of route A are shown in Figure 3. The ^{29}Si NMR peaks for Q^4 and Q^3 of zeolite Beta samples of route A are resolved as two (lines 3 and 4 at −110 and −114 ppm) and one (line 1 at −102 ppm) components, respectively (Figure 3). It should be noted that Q^4(1B) lines are expected to be underneath the Q^4 peak because the chemical shift influence of boron is known to be small.[26] In fact, the line at −110 ppm is reduced after deboronation, which indicates that Q^4(1B) intensity overlaps

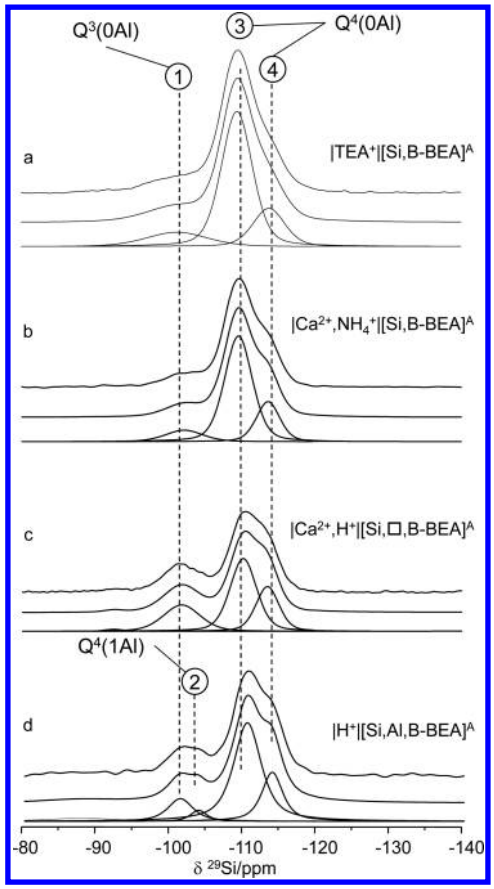

Figure 3. ^{29}Si MAS NMR data of various samples (a−d) and simulations of the spectra; traces are experimental (top), simulated (center), and components (bottom).

with Q^4(0Al) before deboronation. The new line 2 for Q^4(1Al) is found at −104 ppm after Al insertion into the T vacancies, and the Si/Al ratio from the line intensities[43] is 42. Aluminum insertion into the framework defects was successful, and ^{27}Al MAS NMR spectra (Figure S3) in the as-made and calcined forms show that only small amounts of hexacoordinated Al exists after calcination.

The Brønsted acidity was further characterized by thermogravimetric analysis (TGA) and acid-catalyzed fragmentation of isopropylamine (IPA, Figure 4).[44] Four samples were compared in this analysis: $|H^+|[Si,B\text{-}BEA]^A$, i.e., a borosilicate of route A before Al insertion that does not have strong acid sites, and the aluminosilicates $|H^+|[Si,Al\text{-}BEA]^C$, $|H^+|[Si,Al,B\text{-}BEA]^A$, and $|Ca^{2+},H^+|[Si,Al,B\text{-}BEA]^B$. The borosilicate adsorbs 3.0 mmol IPA per g, whereas all aluminosilicates show the same adsorption of 2.7 mmol/g of zeolite. The confirms the structural integrity and comparable porosity of all samples. All samples show a broad peak for physisorbed IPA below 550 K (Figure 4), and three samples have a sharper signal due to the decomposition of chemisorbed IPA formed by protonation at strong Brønsted acid sites. Propene and ammonia were detected in the mass spectrometer upon decomposition of chemisorbed IPA but not for physisorbed IPA (see data for propene in Figure S4). Quantitative analyses of chemisorbed IPA yields the number of acid sites per unit cell (or Si/Al framework ratio for all protonated sites), and the results are shown in Tables 1 and S1, together with Si/Al ratios from ^{29}Si MAS NMR. It should be noted that the weight loss of the chemisorbed IPA was measured up to 723 K because NH_3

DOI: 10.1021/acs.jpcc.6b01680
J. Phys. Chem. C 2016, 120, 9811−9820

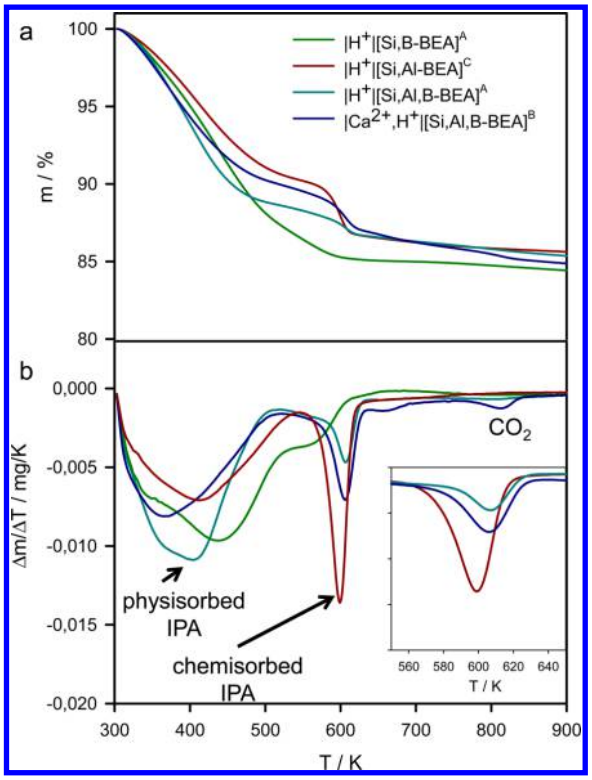

Figure 4. (a) Thermogravimetric and (b) differential thermogravimetric analyses of isopropylamine desorption; inset shows zoom of chemisorbed IPA.

Table 1. Quantitative Analysis of Brønsted Acid Site Concentration and Si/Al Ratios from IPA Decomposition Studies Using TGA and ^{29}Si MAS NMR

sample	IPA TGA Results		^{29}Si MAS NMR
$\|H^+\|[Si,Al,B\text{-}BEA]^A$	1.2 H^+/u.c	Si/Al_{IPA} = 29	Si/Al_{NMR} = 42
$\|Ca^{2+},H^+\|[Si,Al,B\text{-}BEA]^B$	2.3 H^+/u.c.	Si/Al_{IPA} = 19	Si/Al_{NMR} = 31
$\|H^+\|[Si,Al\text{-}BEA]^C$	3.0 H^+/u.c.	Si/Al_{IPA} = 16	Si/Al_{NMR} = 16

formed by IPA decomposition on strong acid sites was observed in the mass spectrometer up to this temperature. This mass loss tailing of the chemisorbed IPA species is likely to be caused by readsorption/desorption processes of NH_3 on strong Brønsted sites during the diffusion through the zeolite channels.

Interestingly, the decomposition peak for chemisorbed IPA of samples A and B appears at 10 K higher than that for sample C. This indicates a higher acidity of the former. The CO_2 peak for sample B is assigned to a carbonate impurity, which is only found in the sample that contained Ca^{2+} ions in the hydrothermal synthesis.

3.2. Quantitative Local H−Al Distance Analyses by ^{1}H−^{27}Al REAPDOR. The ^{1}H−^{27}Al dipolar interaction will now be used to distinguish different local structures and quantify the spin pairing in the different zeolites. The REAPDOR technique developed by Gullion for heteronuclear dipolar interactions with quadrupolar nuclei[45,46] is employed. The protons are measured in two experiments using a spin echo with and without ^{27}Al irradiation. The echo is attenuated by the ^{27}Al pulse, and in principle, this signal loss is directly related to the ^{1}H−^{27}Al dipolar interaction. However, unlike the interaction between two-spin-$^1/_2$ nuclei, the analysis with quadrupolar nuclei is more involved; quantification of the effect is possible only by numerical simulations, especially for large ^{27}Al quadrupolar interactions.[46]

Before experimental results are analyzed, model simulations are shown in Figure 5 to illustrate the major contributions and

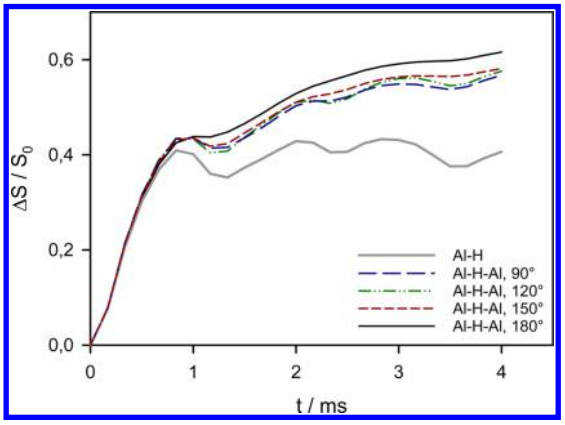

Figure 5. SIMPSON simulations of ^{1}H−^{27}Al REAPDOR evolution curves of ^{1}H−^{27}Al two-spin (Al−H) and ^{1}H−^{27}Al−^{27}Al three-spin systems; Al−H−Al angles in three-spin system are varied (90, 120, 150, and 180°).

influences of ^{1}H−^{27}Al spin systems in zeolites. Various model simulations were carried out with different ^{1}H−^{27}Al dipolar coupling constants, radiofrequency (rf) field strengths, and ^{27}Al quadrupolar interactions. The simulations shown in Figure 5 are selected from a larger set, and they used a first-neighbor dipolar coupling constant of 2000 Hz, a rf field of 50 kHz, and a quadrupolar coupling constant of 16 MHz. An isolated ^{1}H−^{27}Al two-spin pair would be expected to show the oscillating REAPDOR evolution curve labeled "Al−H" in Figure 5. Such oscillations were not observed previously, and we will show below for the first time that it can be found in a zeolite in which acid site isolation is tailored by the synthesis procedure shown above. The oscillation levels at a plateau that is a function of the ^{1}H−^{27}Al heteronuclear dipolar interaction, the rf power (rf field strength), and, to a lesser extent, the ^{27}Al quadrupolar interaction. The positions of minima and maxima of the oscillation also strongly depend on the ^{1}H−^{27}Al dipolar coupling constant. Introducing a third spin, ^{27}Al, with a ^{1}H−^{27}Al dipolar coupling constant of 400 Hz in the simulations will cause two effects: (1) The oscillation is more or less damped depending on the Al−H−Al angle. (2) The oscillation does not remain on a plateau, but the curve shows an additional slope at longer evolution times. The most important consequence of these observations is that interactions between more than two spins will destroy the oscillation part of the REAPDOR evolution, and the curve at longer evolution times will strongly depend on the spin geometry. The latter was previously shown for REDOR of spin-$^1/_2$ systems, which is related to the REAPDOR technique.[47] Therefore, the REAPDOR evolution at longer times contains important information on the size of the spin system and will help identify isolated Brønsted acid sites in zeolites. Fortunately, the oscillatory part of the REAPDOR evolution curve, if it can be observed, is a sensitive and important piece of information on the first ^{1}H−^{27}Al dipolar coupling pair, and it is not affected by other parameters (quadrupolar coupling, rf field, or additional ^{27}Al spin). The simulation of the oscillation leads then to reliable

DOI: 10.1021/acs.jpcc.6b01680
J. Phys. Chem. C 2016, 120, 9811−9820

information on the first H−Al distance, no matter the other influences on the REAPDOR effect.

Experimental ^{1}H−^{27}Al REAPDOR data for |H^{+}|[Si,Al,B-BEA]^{A} reveal large difference intensities observed for the Brønsted protons (4 and 5 ppm) and for hydrogen-bonded extra-framework Al−OH groups (2.8 ppm, Figure 6a). The

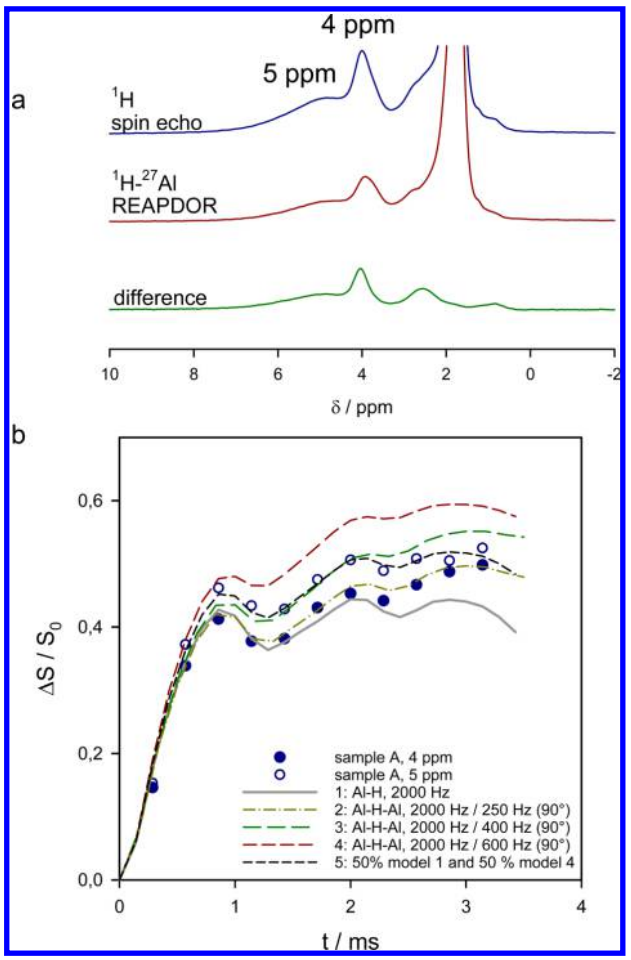

Figure 6. (a) Comparison of ^{1}H spin echo and ^{1}H−^{27}Al REAPDOR at 0.8571 ms evolution time; (b) ^{1}H−^{27}Al REAPDOR evolution of 4 and 5 ppm line of Brønsted acid sites in sample A. Data points were acquired at a spinning frequency of 14 kHz and lines are SIMPSON simulations with various two-spin (Al−H) and three-spin (Al−H−Al) models.

READPOR data points (Figure 6b) of the two Brønsted protons clearly oscillate, and the positions of minima and maxima were simulated with a ^{1}H−^{27}Al dipolar coupling constant of 2000 Hz, which corresponds to a H−Al distance of 2.50 Å. Using other coupling constants and comparing the oscillatory parts of the fits leads to an estimated error of not more than 2% for this H−Al distance. Additionally, the two different protons at 4 and 5 ppm show the same (closest Al−H pair) dipolar coupling constants. This is another indication for the line at 5 ppm not being affected by motion at room temperature in zeolite beta.

However, the REAPDOR curves at longer evolution times cannot be exactly described by isolated two-spin pairs, and it is obvious that the two "plateaus" are not the same. If the nearest H−Al coupling constants are the same for both acid sites, as shown above, then the question arises what causes their difference in the REAPDOR plateaus. Differences in ^{27}Al quadrupolar couplings are very unlikely because this influence is relatively small. The dipolar interaction constant was safely determined from the oscillatory part of the REAPDOR curves for the 4 and 5 ppm lines in Figure 6b. Using a rf field of 52 kHz, as calibrated on the liquid reference sample, lead to a plateau higher than the data points of the 4 ppm line (simulation not shown). This leaves only the rf field as the final parameter to adjust the lower plateau of the REAPDOR curve of the 4 ppm line. Of course, the applied ^{27}Al rf field must be the same for all sites, and it cannot be made accountable for the existence of different REAPDOR plateau levels. However, for decreasing the simulated curve to match with the lower experimental data points of the 4 ppm line, a scaling factor of the rf field seems to be unavoidable, and the higher plateau of the 5 ppm line must then originate from different multiple spin models.

The curves were then simulated with different models based on three-spin dipolar coupling systems to account for the different REAPDOR behavior of the 4 and 5 ppm lines. Selected models (from a larger set investigated) are shown in Figure 6b. The rf field strength (52 kHz), as experimentally determined on a liquid reference sample, was scaled to 49 kHz in the REAPDOR simulations for the zeolite sample. By this means, the lower plateau of the 4 ppm line matches very well with the simulation at short evolution times, but experimental data drift upward at longer evolution. To rationalize why such a scaling factor for the rf field may be permissible, recall that the magnetization generated by a rf excitation pulse depends on the magnetic susceptibility of a sample.[48] Therefore, slightly different rf field uptakes of the zeolite and liquid reference samples are possible. This difference is not unexpected because the NMR probehead tuning often changes when changing samples from the liquid reference to a solid sample and did so here. Measuring the rf field directly on the solid zeolite sample was impossible because of the extreme broadness of the signal of acid sites. Because the rf field strength is of considerable importance for the REAPDOR curve plateau, this parameter is critical for quantitative analysis.

The line at 4 ppm can be described best by a Al−H−Al three-spin system for the entire evolution period with a first dipolar coupling constant of 2000 Hz (2.50 Å) and a second one of 250 Hz (5.00 Å) with a Al−H−Al angle of 90°. In addition to an interaction within the same pore, such a second H−Al distance is, for example, also possible if the proton in one zeolite beta channel interacts with ^{27}Al in a neighboring channel. The line at 5 ppm is more difficult to simulate. A "simple" three-spin system did not work in all cases. It was not possible to describe the relatively small slope at evolution times beyond 2 ms by a three-spin site. A bimodal model is more successful, and the best fit in Figure 6b is a 1:1 contribution of an isolated ^{1}H−^{27}Al two spin pair (2000 Hz) and a ^{27}Al−^{1}H−^{27}Al three-spin system (2000 and 600 Hz), corresponding to distances of 2.50 and 3.73 Å. A second distance at 3.73 Å, for example, is geometrically possible within the same six-ring (if B is replaced by Al in Figure 1b). In summary, the line at 4 ppm is a reasonably isolated acid site, and the closest next Al neighbor is at a distance of 5 Å. The 5 ppm line is assigned to protons, which are either isolated or paired with an aluminum nearby for example in the same six-ring (bimodal 1:1 model).

The REAPDOR analyses of sample C before, |Na^{+},H^{+}|[Si,Al-BEA]^{C}, and after NH_4^{+} ion exchange, |H^{+}|[Si,Al-BEA]^{C}, show

DOI: 10.1021/acs.jpcc.6b01680
J. Phys. Chem. C 2016, 120, 9811−9820

different behavior (Figure 7). No clear oscillation is detected for the experimental data points, and it is difficult to simulate

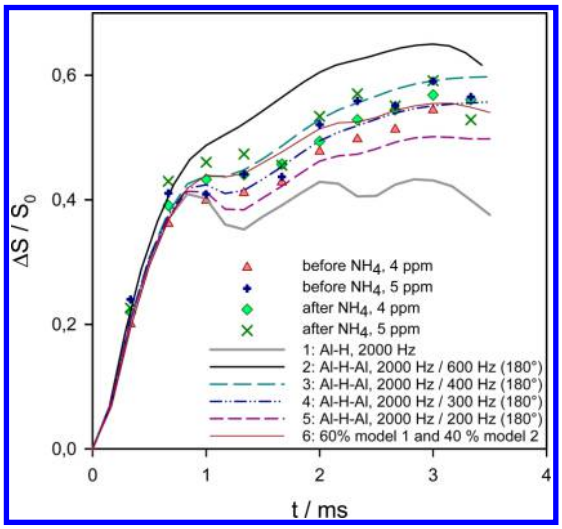

Figure 7. $^{1}H-^{27}Al$ REAPDOR evolution of 4 and 5 ppm line of Brønsted acid sites in sample C before and after NH_4^+ exchange (rotation with 12 kHz); lines are SIMPSON simulations with various models.

the REAPDOR evolution curves with a simple two- or three-spin model with the same confidence as for sample A. This is a clear indication for sample C that multiple-spin interactions and/or multimodal spin systems may contribute to the curves beyond the initial slope region of the REAPDOR evolution at 1 ms or longer times. A first H−Al distance of 2.50 Å (2000 Hz dipolar coupling constant) and at least another ^{27}Al spin with various coupling models appears to be in a reasonable range to explain the REAPDOR evolution of these samples. A reasonable fit for the 4 ppm line after NH_4^+ exchange can be achieved by a bimodal model with 60% Al−H two-spin pairs and 40% Al−H−Al (2000/600 Hz) three-spin systems. However, the agreement in Figure 7 is less satisfactory than the models shown in Figure 6, and it is concluded that sample C does not contain truly isolated (or well-defined pairing of) acid sites.

Figure 8 summarizes model structures that are in agreement with the REAPDOR analysis of sample $|H^+|[Si,Al,B\text{-}BEA]^A$. These proposed models were obtained by using six-ring structures of polymorph A of zeolite beta[49] and manually placing H atoms at selected positions which are rationalized by the quantitative distance data of this work. Hydrogen-bonded acid protons are likely to occur in ring positions, where the oxygen atoms are directed with their (negative) Si−O−Al vector direction toward an oxygen on the opposite side of the ring, or, in other words, where large T−T−O−O torsion angles are observed. For example, this is the case for the T5−T3−O10 → O13 torsion angle of 162.4°, which was used to construct the H-bonded models. However, the T6−T8−O16 →O12 torsion angle (128.1°) indicates that O16 points more into the channel center rather than into the six-ring. This was used for the non-H-bonded model in Figure 8. Distances of 2.50 and 3.73 Å can be well-explained by six-ring structures, but a H−Al distance of 5.0 Å is too large to be found in the same six-ring. Therefore, the line at 4 ppm of sample A is considered an isolated site because it has a second Al neighbor only outside of a six-ring, possibly in the neighboring channel. The 5 ppm line

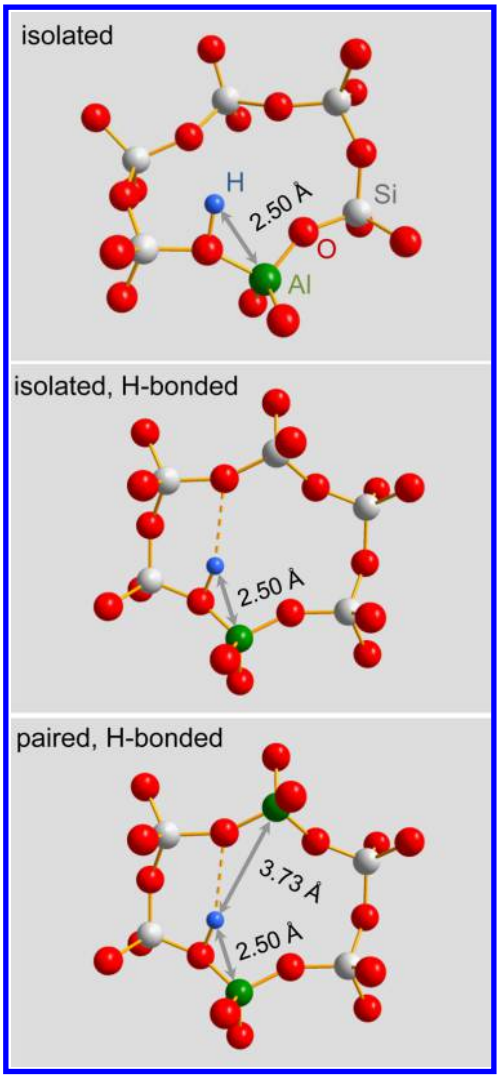

Figure 8. Survey of reasonable six-ring models to the best fits of $^{1}H-^{27}Al$ distance analyses of sample $|H^+|[Si, Al,B\text{-}BEA]^A$; the isolated proton ($\delta$ = 4 ppm) has a second Al neighbor at 5 Å (not shown), which could be in a neighboring channel. H-bonded proton (δ = 5 ppm) is best described by a bimodal model with 50% isolated and 50% paired sites; ring structures were taken from polymorph A of zeolite beta.

is explained by a 1:1 combination of two structures: an isolated H-bonded site and a paired H-bonded site.

4. CONCLUSIONS

Borosilicate zeolites allow tailored postsynthesis modification by tuning the boron reactivity with different charge-balancing counterions. In the proton form, boron is easily extracted by water treatment. More ionic charge-balancing cations, such as Ca^{2+} (or Na^+) serve as protecting agents in a nonaqueous ion exchange which avoids undesired boron leaching, for example, by using methanol as solvent. A mixed nonaqueous ion exchange with Ca^{2+} and NH_4^+ allows tailoring of the subsequent aqueous boron extraction by tuning the reactivity of framework boron by the binding affinity of the cations, ionic Ca^{2+} versus covalent H^+ formed from NH_4^+ by calcination. After Al insertion into the hydroxyl nests generated by boron extraction, strong acid sites are formed.

DOI: 10.1021/acs.jpcc.6b01680
J. Phys. Chem. C 2016, 120, 9811−9820

For the first time, an oscillation of the $^{1}H-^{27}Al$ heteronuclear dipolar REAPDOR evolution curves could be simulated quantitatively in a zeolite acid site. Nearest H−Al distances were determined at 2.50 Å with an accuracy at least as good as 2% on the basis of the oscillation part of the REAPDOR curves. Second nearest Al neighbors were either relatively far away at 5 Å for the acid site with δ_{1H} = 4 ppm, for example, in a neighboring channel, or a second Al neighbor, for example, in the same six-ring, only occurs for about 50% of the sites at δ_{1H} = 5 ppm. Therefore, heteronuclear $^{1}H-^{27}Al$ dipolar interactions may be used as a novel tool to determine the Al distribution in zeolite frameworks.

■ ASSOCIATED CONTENT

Supporting Information

The Supporting Information is available free of charge on the ACS Publications website at DOI: 10.1021/acs.jpcc.6b01680.

Adsorption data of isopropylamine, XRD data of various samples of routes A−C, ^{27}Al MAS NMR of various samples (routes A and B) after Al insertion, and temperature-dependent propene mass flux (m/e = 39) as observed in the mass spectrometer after heating in the TGA. (PDF)

■ AUTHOR INFORMATION

Corresponding Author

*E-mail: hubert.koller@uni-muenster.de. Phone: +49 251 8323448. Fax: +49 251 8323409.

Notes

The authors declare no competing financial interest.

■ ACKNOWLEDGMENTS

We thank Julia Zimdars for help in ^{1}H NMR simulations and Sascha Nowak for chemical analyses. S.S. thanks the Graduate School of Chemistry for a fellowship. This paper is dedicated to Prof. Günter Engelhardt on the occasion of his 80th birthday.

■ REFERENCES

(1) Kühl, G. H. Modification of Zeolites. In *Catalysis and Zeolites*; Weitkamp, J.; Puppe, L., Eds.; Springer: Berlin, 1999; pp 81−197.

(2) van Bekkum, H.; Flanigen, E.M.; Jacobs, P.A.; Jansen, J. C. *Introduction to Zeolite Science and Practice*; Elsevier Science B.V.: Amsterdam, 2001.

(3) Tatsumi, T. Modification of Crystalline Microporous Solids. In *Handbook of Porous Solids*; Schüth, F.; Sing, K. S. W.; Weitkamp, J., Eds.; Wiley-VCH: Weinheim, 2002; Vol. 2, pp 903−935.

(4) Chen, C. Y.; Zones, S. I. Post-Synthetic Treatment and Modification of Zeolites. In *Zeolites and Catalysis*; Čejka, J.; Corma, A.; Zones, S., Eds.; Wiley-VCH Verlag GmbH & Co. KGaA: Weinheim, 2010; pp 155−170.

(5) Csicsery, S. M. Catalysis by Shape Selective Zeolites - Science and Technology. *Pure Appl. Chem.* **1986**, *58*, 841−856.

(6) Marcilly, C. R. Where and How Shape Selectivity of Molecular Sieves Operates in Refining and Petrochemistry Catalytic Processes. *Top. Catal.* **2000**, *13*, 357−366.

(7) Perego, C.; Calemma, V.; Pollesel, P., Naphtha Reforming and Upgrading of Diesel Fractions. In *Zeolites and Catalysis*; Čejka, J.; Corma, A.; Zones, S. I., Eds.; Wiley-VCH: Weinheim, 2010; Vol. 2, pp 585−621.

(8) Davis, M. E. Catalytic Materials Via Molecular Imprinting. *CATTECH* **1997**, *1*, 19−26.

(9) Gorte, R. J. Surface Acidity. In *Handbook of Porous Solids*; Schüth, F.; Sing, K. S. W.; Weitkamp, J., Eds.; Wiley-VCH: Weinheim, 2002; Vol. 1, pp 432−464.

(10) Gounder, R.; Iglesia, E. Effects of Partial Confinement on the Specificity of Monomolecular Alkane Reactions for Acid Sites in Side Pockets of Mordenite. *Angew. Chem., Int. Ed.* **2010**, *49*, 808−811.

(11) Gounder, R.; Iglesia, E. The Roles of Entropy and Enthalpy in Stabilizing Ion-Pairs at Transition States in Zeolite Acid Catalysis. *Acc. Chem. Res.* **2012**, *45*, 229−238.

(12) Koller, H.; Engelhardt, G.; van Santen, R. A. The Dynamics of Hydrogen Bonds and Proton Transfer in Zeolites - Joint Vistas from Solid-State NMR and Quantum Chemistry. *Top. Catal.* **1999**, *9*, 163−180.

(13) Hunger, M. Catalytically Active Sites: Generation and Characterization. In *Zeolites and Catalysis*; Čejka, J.; Corma, A.; Zones, S. I., Eds.; Wiley-VCH: Weinheim, 2010; Vol. 2, pp 493−546.

(14) Savitz, S.; Siperstein, F.; Gorte, R. J.; Myers, A. L. Calorimetric Study of Adsorption of Alkanes in High-Silica Zeolites. *J. Phys. Chem. B* **1998**, *102*, 6865−6872.

(15) Ertl, G.; Knözinger, H.; Schüth, F.; Weitkamp, J. *Handbook of Heterogeneous Catalysis*; Wiley-VCH: Weinheim, 2008; Vol. 3.

(16) Satsuma, A.; Shichi, A.; Hattori, T. The Zeolite Micropore as a Unique Reaction Field for the Selective Catalytic Reduction of NO by Hydrocarbon. *CATTECH* **2003**, *7*, 42−51.

(17) Kärger, J.; Ruthven, D. M.; Theodorou, D. N. *Diffusion in Nanoporous Materials*; Wiley-VCH: Weinheim, 2012.

(18) Dedecek, J.; Sobalik, Z.; Wichterlova, B. Siting and Distribution of Framework Aluminium Atoms in Silicon-Rich Zeolites and Impact on Catalysis. *Catal. Rev.: Sci. Eng.* **2012**, *54*, 135−223.

(19) Sklenak, S.; Dědeček, J.; Li, C. B.; Wichterlová, B.; Gábová, V.; Sierka, M.; Sauer, J. Aluminum Siting in Silicon-Rich Zeolite Frameworks: A Combined High-Resolution ^{27}Al NMR Spectroscopy and Quantum Mechanics/Molecular Mechanics Study of ZSM-5. *Angew. Chem., Int. Ed.* **2007**, *46*, 7286−7289.

(20) Dědeček, J.; Sklenak, S.; Li, C.; Wichterlová, B.; Gábová, V.; Brus, J.; Sierka, M.; Sauer, J. Effect of Al-Si-Al and Al-Si-Si-Al Pairs in the ZSM-5 Zeolite Framework on the ^{27}Al NMR Spectra. A Combined High-Resolution ^{27}Al NMR and DFT/MM Study. *J. Phys. Chem. C* **2009**, *113*, 1447−1458.

(21) Koller, H.; Meijer, E. L.; van Santen, R. A. ^{27}Al Quadrupole Interaction in Zeolites Loaded with Probe Molecules - a Quantum-Chemical Study of Trends in Electric Field Gradients and Chemical Bonds in Clusters. *Solid State Nucl. Magn. Reson.* **1997**, *9*, 165−175.

(22) Kentgens, A. P. M.; Iuga, D.; Kalwei, M.; Koller, H. Direct Observation of Bronsted Acidic Sites in Dehydrated Zeolite H-ZSM5 Using DFS-Enhanced ^{27}Al MQMAS NMR Spectroscopy. *J. Am. Chem. Soc.* **2001**, *123*, 2925−2926.

(23) Pashkova, V.; Klein, P.; Dedecek, J.; Tokarova, V.; Wichterlova, B. Incorporation of Al at ZSM-5 Hydrothermal Synthesis. Tuning of Al Pairs in the Framework. *Microporous Mesoporous Mater.* **2015**, *202*, 138−146.

(24) Millini, R.; Perego, G.; Bellussi, G. Synthesis and Characterization of Boron-Containing Molecular Sieves. *Top. Catal.* **1999**, *9*, 13−34.

(25) Chen, C. Y.; Zones, S. I. From Borosilicate to Gallo- and Aluminosilicate Zeolites: New Methods for Lattice Substitution Via Post-Synthetic Treatment. *Stud. Surf. Sci. Catal.* **2001**, *135*, 1710−1717.

(26) Koller, H.; Chen, C. Y.; Zones, S. I. Selectivities in Post-Synthetic Modification of Borosilicate Zeolites. *Top. Catal.* **2015**, *58*, 451−479.

(27) Hough, A.; Routh, A. F.; Clarke, S. M.; Wiper, P. V.; Amelse, J. A.; Mafra, L. Boron Removal and Reinsertion Studies in B-10-B-11 Exchanged HAMS-1B (H-[B]-ZSM-5) Borosilicate Molecular Sieves Using Solid-State NMR. *J. Catal.* **2016**, *334*, 14−22.

(28) Xie, D.; McCusker, L. B.; Baerlocher, C. Structure of the Borosilicate Zeolite Catalyst SSZ-82 Solved Using 2D-XPD Charge Flipping. *J. Am. Chem. Soc.* **2011**, *133*, 20604−20610.

(29) Xie, D.; McCusker, L. B.; Baerlocher, C.; Gibson, L.; Burton, A. W.; Hwang, S. J. Optimized Synthesis and Structural Characterization of the Borosilicate MCM-70. *J. Phys. Chem. C* **2009**, *113*, 9845−9850.

DOI: 10.1021/acs.jpcc.6b01680
J. Phys. Chem. C 2016, 120, 9811−9820

(30) Grünewald-Lüke, A.; Gies, H.; Müller, U.; Yilmaz, B.; Imai, H.; Tatsumi, T.; Xie, B.; Xiao, F.-S.; Bao, X. H.; Zhang, W.; De Vos, D. Layered Precursors for New Zeolitic Materials: Synthesis and Characterization of B-RUB-39 and Its Condensation Product B-RUB-41. *Microporous Mesoporous Mater.* **2012**, *147*, 102−109.
(31) Tong, H. T. T.; Koller, H. Control of Al for B Framework Substitution in Zeolite Beta by Counterions. *Microporous Mesoporous Mater.* **2012**, *148*, 80−87.
(32) Van Nordstrand, R. A.; Santilli, D. S.; Zones, S. I. Aluminum- and Boron-Containing SSZ-24: Inverse Shape Selectivity in the AFI Structure. In *Synthesis of Microporous Materials*; Occelli, M. L.; Robson, H. E., Eds.; Van Nostrand Reinhold: New York, 1992; Vol. *I*, pp 373−383.
(33) Zones, S. I.; Benin, A.; Hwang, S. J.; Xie, D.; Elomari, S.; Hsieh, M. F. Studies of Aluminum Reinsertion into Borosilicate Zeolites with Intersecting Channels of 10-and 12-Ring Channel Systems. *J. Am. Chem. Soc.* **2014**, *136*, 1462−1471.
(34) Senapati, S.; Zimdars, J.; Ren, J.; Koller, H. Post-Synthetic Modifications of as-Made Zeolite Frameworks near the Structure-Directing Agents. *J. Mater. Chem. A* **2014**, *2*, 10470−10484.
(35) Bak, M.; Rasmussen, J. T.; Nielsen, N. C. Simpson: A General Simulation Program for Solid-State NMR Spectroscopy. *J. Magn. Reson.* **2000**, *147*, 296−330.
(36) Beck, L. W.; Haw, J. F. Multinuclear Nmr-Studies Reveal a Complex Acid Function for Zeolite-Beta. *J. Phys. Chem.* **1995**, *99*, 1076−1079.
(37) Beck, L. W.; White, J. L.; Haw, J. F. ^{1}H-^{27}Al Double-Resonance Experiments in Solids - an Unexpected Observation in the ^{1}H Mas Spectrum of Zeolite HZSM-5. *J. Am. Chem. Soc.* **1994**, *116*, 9657−9661.
(38) Eichler, U.; Brändle, M.; Sauer, J. Predicting Absolute and Site Specific Acidities for Zeolite Catalysts by a Combined Quantum Mechanics Interatomic Potential Function Approach. *J. Phys. Chem. B* **1997**, *101*, 10035−10050.
(39) Sillar, K.; Burk, P. Hybrid Quantum Chemical and Density Functional Theory (ONIOM) Study of the Acid Sites in Zeolite ZSM-5. *J. Phys. Chem. B* **2004**, *108*, 9893−9899.
(40) Huo, H.; Peng, L.; Grey, C. P. Low Temperature ^{1}H MAS NMR Spectroscopy Studies of Proton Motion in Zeolite HZSM-5. *J. Phys. Chem. C* **2009**, *113*, 8211−8219.
(41) Fenzke, D.; Hunger, M.; Pfeifer, H. Determination of Nuclear Distances and Chemical-Shift Anisotropy from ^{1}H MAS NMR Side-Band Patterns of Surface OH Groups. *J. Magn. Reson.* **1991**, *95*, 477−483.
(42) Hunger, M.; Freude, D.; Fenzke, D.; Pfeifer, H. ^{1}H Solid-State NMR-Studies of the Geometry of Bronsted Acid Sites in Zeolites H-ZSM-5. *Chem. Phys. Lett.* **1992**, *191*, 391−395.
(43) Engelhardt, G.; Michel, D. *High-Resolution Solid-State NMR of Silicates and Zeolites*; John Wiley & Sons: Chichester, 1987.
(44) Farneth, W. E.; Gorte, R. J. Methods for Characterizing Zeolite Acidity. *Chem. Rev.* **1995**, *95*, 615−635.
(45) Gullion, T. Measurement of Dipolar Interactions between Spin-1/2 and Quadrupolar Nuclei by Rotational-Echo, Adiabatic-Passage, Double-Resonance NMR. *Chem. Phys. Lett.* **1995**, *246*, 325−330.
(46) Gullion, T.; Vega, A. J. Measuring Heteronuclear Dipolar Couplings for I = 1/2, S > 1/2 Spin Pairs by REDOR and REAPDOR NMR. *Prog. Nucl. Magn. Reson. Spectrosc.* **2005**, *47*, 123−136.
(47) Bertmer, M.; Eckert, H. Dephasing of Spin Echoes by Multiple Heteronuclear Dipolar Interactions in Rotational Echo Double Resonance NMR Experiments. *Solid State Nucl. Magn. Reson.* **1999**, *15*, 139.
(48) Abragam, A. *Principles of Nuclear Magnetism*; Oxford Science Publications: Oxford, 1961.
(49) Baerlocher, C.; McCusker, L. B. *Database of Zeolite Structures*. http://www.iza-structure.org/databases/ (accessed on April 12, 2016).

DOI: 10.1021/acs.jpcc.6b01680
J. Phys. Chem. C 2016, 120, 9811−9820